aerospace

MDPI

Article

Design and Structural Analyses of a Reciprocating S1223 High-Lift Wing for an RA-Driven VTOL UAV

Johnson O. Imumbhon *, Mohammad D. Alam and Yiding Cao

Department of Mechanical and Materials Engineering, Florida International University, Miami, FL 33174, USA; malam052@fiu.edu (M.D.A.); caoy@fiu.edu (Y.C.)
* Correspondence: jimum001@fiu.edu

Abstract: In the design stage of an aircraft, structural analyses are commonly employed to test the integrity of the aircraft components to demonstrate the capability of the structural elements to withstand what they are designed for, as well as predict potential failure of the components. This research focused on the structural design and analysis of a high-lift, low Reynolds number airfoil profile, the Selig S1223, under reciprocating inertial force loading, to determine the feasibility of its use in a new reciprocating airfoil (RA) driven VTOL UAV. The material selected for the wing structures including ribs, spars, and skin, was high-strength carbon fiber. The wing was designed in SolidWorks, while finite element analysis was performed with ANSYS mechanical in conjunction with the inertia forces due to the reciprocating motion of the wing and the lift and drag forces that were derived from the aerodynamic wing analyses. The structural stress and strain determined under the loading conditions were satisfactory and the designed wing could sustain the high reciprocating inertia forces in the RA-driven VTOL UAV module. The results of this study indicate that the Selig S1223 airfoil profile, due to its superior performance at low Reynolds numbers, high-lift, and reduced noise characteristics at low angles of attack, combined with the use of the high strength carbon fiber, proves to be an excellent choice for this RA-driven aircraft application.

Keywords: high-lift; reciprocating airfoil; S1223; stress analysis; VTOL UAV module

Citation: Imumbhon, J.O.; Alam, M.D.; Cao, Y. Design and Structural Analyses of a Reciprocating S1223 High-Lift Wing for an RA-Driven VTOL UAV. *Aerospace* **2021**, *8*, 214. https://doi.org/10.3390/aerospace8080214

Academic Editor: Lance Traub

Received: 26 June 2021
Accepted: 30 July 2021
Published: 5 August 2021

1. Introduction

Since the invention of the aircraft, traveling by air using fixed-wing airplanes has remained the safest means of transportation. However, the current trend of aircraft development is in the area of unmanned aerial vehicles (UAVs), especially those that can perform vertical takeoff and landing (VTOL) operations. This has given rise to current and potential solutions for the new needs of both military and civilian applications.

Over recent years, various kinds of UAV concepts have been developed [1–12]. The three most common types of UAVs are the rotary-wing UAVs, the fixed-wing (FW) UAVs, and the mixed UAVs known as hybrid UAVs. Rotary-wing UAVs generate lift with rotary blades or multiple rotors. Examples of rotary-wing UAVs include the Northrop Grumman MQ-8C Fire Scout and the VSR700 from Airbus (currently under development), which are respectively shown in Figure 1a [1] and Figure 1b [2]. The addition of extra blades/rotors, thrust engines, and wings (usually near the tail end of traditional rotary-wing aircraft) to rotary-wing vehicles results in a new group of aircraft known as compound aircraft. These compound aircraft can attain a top speed of up to 487 km/h. An example of a compound aircraft is the Sikorsky-Boeing SB >1 Defiant [13].

(**a**) (**b**)

Figure 1. Examples of Rotary UAV systems: (**a**) The Airbus VSR700. Photo courtesy of Airbus [1], (**b**) The Northrop Grumman MQ-8C Fire Scout. Photo courtesy of Northrop Grumman [2].

Fixed-wing UAVs are the most developed and normally receive the most funding from the military because of their numerous benefits, such as longer flight durations, higher speeds, and endurance when compared to other kinds of UAVs. Examples of high-end FW UAVs are the Northrop Grumman RQ-4 Global Hawk, as shown in Figure 2 [3], and the General Atomics MQ-9 Reaper [4]. However, fixed-wing UAVs may be generally costly, do not possess vertical lift and hovering capabilities, and usually require runways or a take-off platform for takeoff and landing.

Figure 2. Example of a fixed-wing UAV: The Northrop Grumman RQ-4. Photo courtesy of Northrop Grumman [3].

Another alternative is the hybrid UAVs that combine the vertical flight capability of rotary wings or fans with fixed wings to carry out various missions. The two broad categories of hybrid UAVs are tail-sitters and convertiplanes. Tail-sitters take off and land vertically on the tail, while convertiplanes can perform VTOL operations and transition to a fixed-wing flight mode. Convertiplanes can be categorized into four main types, namely: Tilt-wing, Tilt-rotor, Stop-rotor (or Rotor-wing), and Dual-system. Two examples of hybrid UAVs are the TURAC VTOL UAV [5] and the quad tilt-wing UAV [6], as shown in Figure 3a,b, respectively. The TURAC VTOL UAV concept has detachable and interchangeable wings that can perform a vertical lift and conventional takeoff and landing (CTOL) [5]. The quad tilt-wing UAV uses a plurality of relatively small fans to provide lift during takeoff and landing and turns the fans by 90 degrees to work as propellers during the cruise [6].

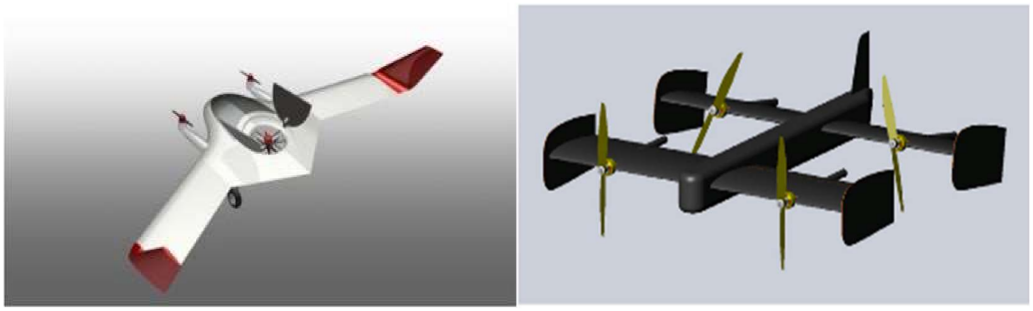

(**a**) (**b**)

Figure 3. Examples of hybrid UAVs: (**a**) The TURAC VTOL UAV. Reprinted from [5], (**b**) The SUAVI quad tilt-wing UAV. Reprinted from [6].

Most of the VTOL UAVs currently being developed utilize rotary wings like those used in conventional helicopters, or small fans to provide lift during takeoff and landing. However, the use of rotary wings may inherit the challenges of having relatively low energy efficiency, limited flight speed and flight range, and safety issues associated with conventional helicopters. The use of small fans as a means of lift may be convenient and easy to control, but a fan can only produce very limited lift as compared to the rotary-wing of a helicopter. By realizing the above challenges, a new aircraft, the reciprocating-airfoil (RA) driven VTOL aircraft, has been conceived [14,15].

The reciprocating airfoil (RA) works in cycles, each including a forward and a reverse stroke (Figure 4). The airfoil moves back and forth within a sufficiently long stroke, and near each dead-end of the stroke, it is actuated to rotate at an angle while reversing the direction with a positive effective angle of attack (AoA) to produce lift. The reciprocating wing is shaped like a fixed-wing and produces lift for vertical takeoff and landing as well as hovering. During the cruise, however, the wing can stop the reciprocating motion and function as a fixed-wing, with its operation attaining the performance of the fixed-wing of a conventional airplane. An RA-based aircraft is thus, a natural extension of a fixed-wing aircraft with similar cruise performance, but with an added capability for vertical takeoff and landing. To cancel the inertia forces and moments of individual airfoils, RAs can be deployed in modules, each including two wings that reciprocate simultaneously with the same velocity magnitude but in opposite directions.

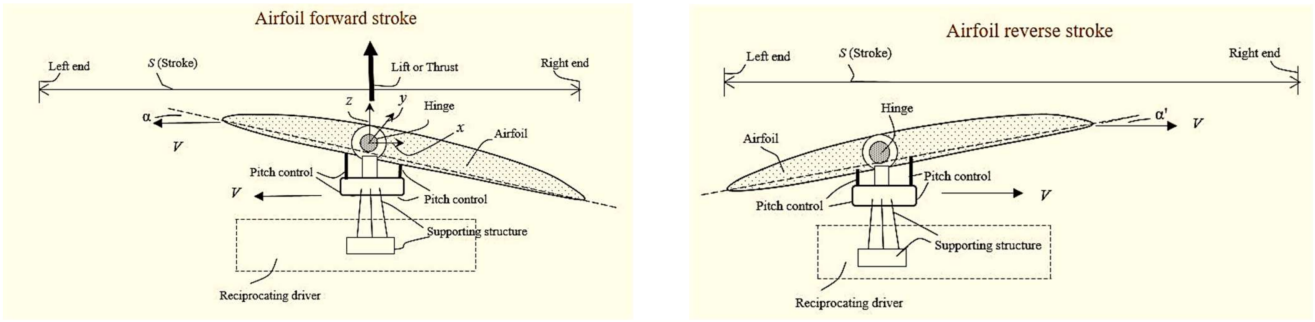

(**a**) (**b**)

Figure 4. Schematic illustration of a reciprocating wing cycle. Reprinted from [14]: (**a**) Forward stroke and (**b**) Reverse stroke.

Although the RA module may provide both lift and thrust, Figure 5 shows an RA-driven VTOL aircraft using an RA module for lift and a propeller for thrust, which is a snapshot of the operational animation of a SolidWorks conceptual design. During takeoff, most of the power is used to drive the RA module. Because the reciprocating motion of the RA wings is largely linear and the wings have a similar shape to fixed wings, the

reciprocating wings can have the capability to produce a large lift, approaching that of fixed wings and exceeding the lift of rotary wings. Once the aircraft is in the air, the propeller is turned on and the cruise speed of the aircraft increases. The power gradually shifts to the propeller, accompanied by a gradual reduction in the reciprocating speed of the RA module. The cruise speed of the aircraft creates airflow through the RA module to produce lift and the need for the reciprocating motion of the RA module is reduced. At a sufficiently high flight speed (around 240 km/h), the RA module will completely stop reciprocating and function as fixed wings for lift. The transitions from the takeoff mode to the fixed-wing flight mode are smooth and natural because of the superposition of the airflow speed due to the aircraft cruise speed, and the speed due to the reciprocating motion of the wings. The high lift capability during takeoff and the smooth and natural transition to the fixed-wing operation represents the most unique advantages of the RA aircraft, that all other VTOL aircraft, including turn-rotator aircraft, may not be able to match. For a more detailed description of the RA VTOL aircraft, please see Cao [14,15]. The objective of this study was to structurally determine the feasibility of the reciprocating wing in an RA aircraft-based VTOL UAV model.

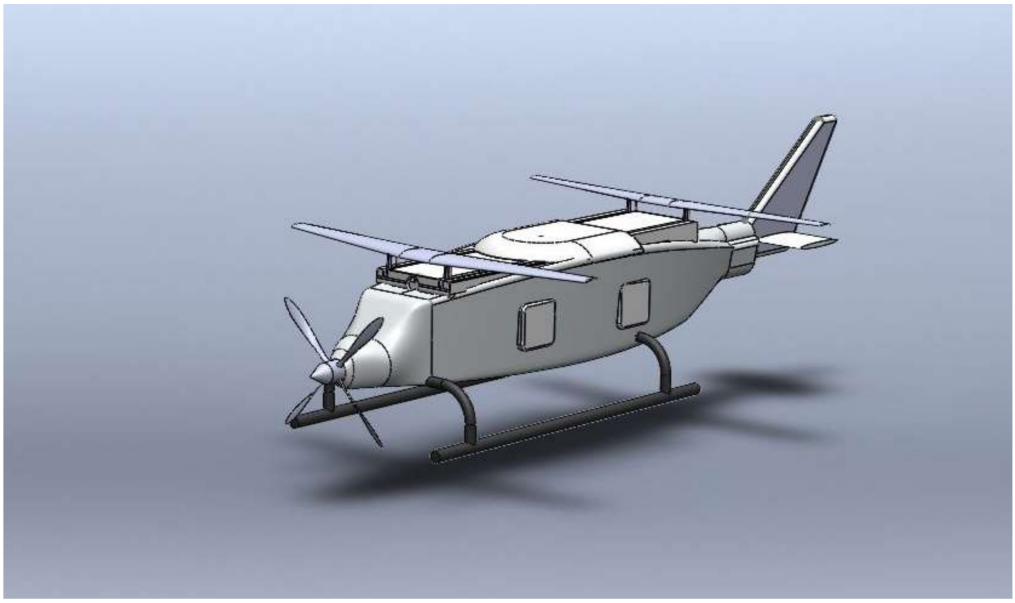

Figure 5. A snapshot of the animation of a SolidWorks conceptual design of an RA-driven VTOL aircraft.

2. The Reciprocating Airfoil (RA) Driven VTOL Drone Model

Based on the concept of the RA-driven VTOL aircraft [14], an RA-driven VTOL UAV drone model was designed, which is the core of an RA-driven VTOL aircraft. Figure 6 is a schematic design including the essential structures of an RA drone for urban goods deliveries. Two wings are deployed in the RA module that reciprocates simultaneously with the same magnitude of velocity but in opposite directions. This is to cancel the inertia forces and moments of the individual airfoils. The aircraft wing can be driven by a crankshaft, hydraulic, electric, or electromagnetic driver. The crankshaft is chosen for the RA module because of the advantage of converting rotary motion into a reciprocating motion with the loss of energy only related to friction, and the capability to produce longer strokes for the wings. The crankshaft mechanism that produces the reciprocating motion of the RA wings is driven by a battery pack.

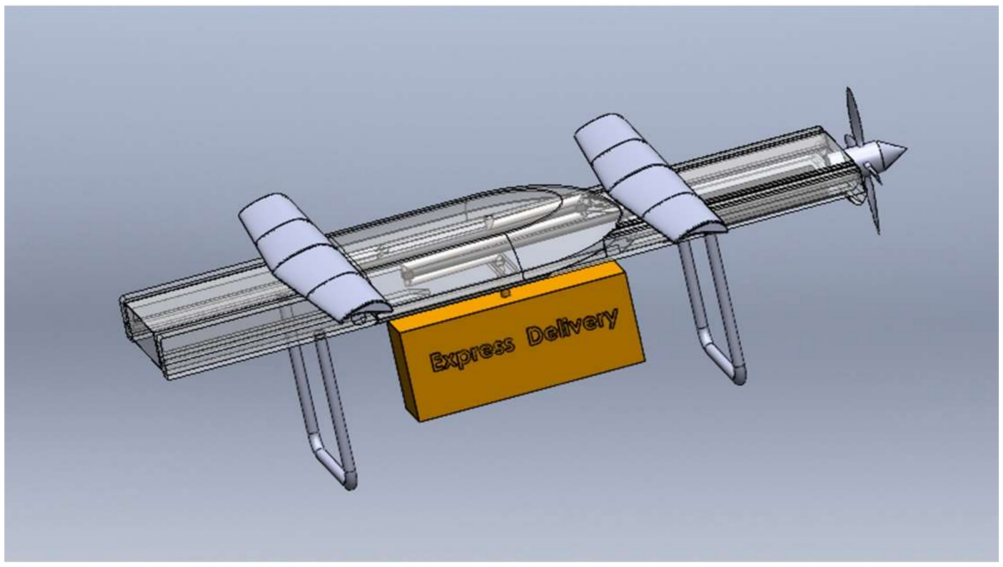

Figure 6. Schematic of a Reciprocating-Wing Driven VTOL UAV Model.

2.1. Airfoil Selection and RA Validation

Selecting the appropriate parameters of an airfoil profile for wing design is usually based on performance data, computational fluid dynamics (CFD) calculations, statistics, or historical usage. The three general classes of airfoils are general-purpose, high-lift, and high-speed airfoils. The general-purpose airfoil has sharper leading edges and a lower thickness ratio, whereas high-lift airfoils have rounded leading edges with a thicker ratio and are more suited for short field aircraft operations and sailplanes. The high-speed airfoils have the smallest thickness with sharp leading edges and are mostly used for high-speed aircraft. The shape and size of the airfoil usually dictate the application environment where it will operate. Furthermore, the airfoil profile that forms the aircraft wing directly affects the lift, stall speed (slowest speed an aircraft can fly to maintain a level flight), and general aerodynamic efficiency. The stall characteristics, thickness, pitching moments, high-lift, airfoil lift-to-drag ratio are all important features in the selection of an airfoil.

Figure 7 shows the Selig S1223 (named after Michael Selig) airfoil profile selected for this study. The S1223 has been studied by researchers for applications of high-lift and relatively low flight speeds and tested with more sophisticated equipment than when most NACA (National Advisory Committee for Aeronautics) airfoils were created.

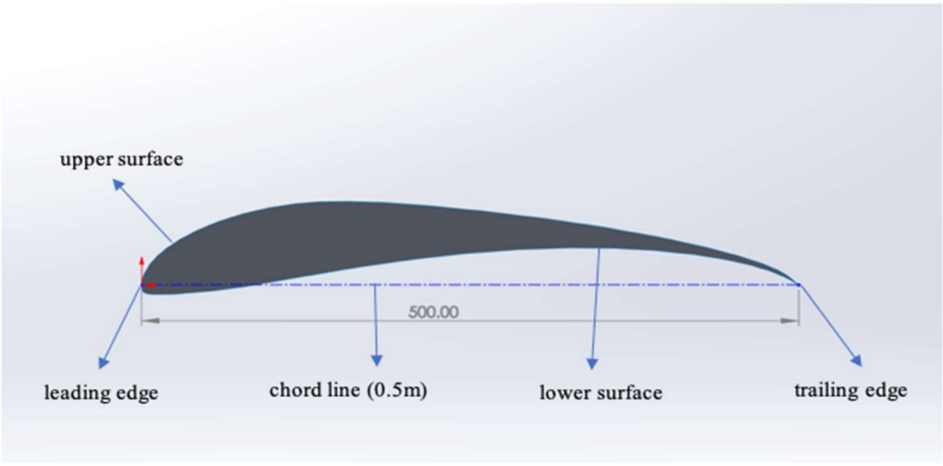

Figure 7. A standard Selig S1223 Airfoil (wing root) profile.

Most airfoil models operate in the low Reynolds number range between 1×10^5 and 1×10^6 including both laminar and turbulent flows, and unmanned aerial vehicles (UAVs) usually operate in the 2×10^5 to 5×10^5 Reynolds number range. The S1223 is considered to be a high-lift and low Reynolds number airfoil that is suitable for short field aircraft operations. It has a reduced noise characteristic at low AoA and is suitable for a shortened takeoff and landing with an increased payload. These characteristics of the S1223 have been validated through wind tunnel testing as the most suitable airfoil for a low Reynolds number UAV [16]. Even when the fluid is water, the S1223 airfoil profile is very suitable for hydrodynamic tasks, particularly for a hydrokinetic turbine blade design [17]. For the present RA VTOL application, the same airfoil is used as both the reciprocating wing during the takeoff and fixed-wing during the cruise. During the takeoff, the reciprocating speed is relatively low but requires a high lift. For the present UAV application, the cruise speed should also be relatively low, which would satisfy the low Reynolds number condition. Because of the numerous advantages coupled with our needs, the S1223 was chosen as the wing profile for the RA-driven VTOL UAV.

2.2. Aerodynamic Properties and Computational Fluid Dynamics (CFD) Results of the S1223 Airfoil Profile

The aerodynamic lift performance results from a selection of low Reynolds number airfoils, including M06-13-128, FX 63-137, LNV109A, E214, S1223, E423, and LA2573A, show that the S1223 outperforms other good airfoils at low Reynolds numbers [18]. Table 1 shows some performance data of the S1223 and Figure 8a is a plot of the S1223 lift coefficient (C_L) versus the AoA as a fixed airfoil, which indicates that the maximum airfoil coefficient of lift at a Reynolds number of 2×10^5, is approximately 2.23 [16]. Figure 8b shows some 3D CFD results of an S1223 reciprocating wing for the lift and drag at different aircraft flight speeds.

Table 1. Aerodynamic properties and the CFD results from analysis of the S1223 airfoil profile. Adapted from [16,17].

Airfoil Name	S1223
Stall Angle	14
$C_{L,max}$ at Re = 2.0×10^5	2.23
α_{max} (degrees)	15
$C_{m,c/4}$	−0.29
Relative thickness (blade root)	12.13%

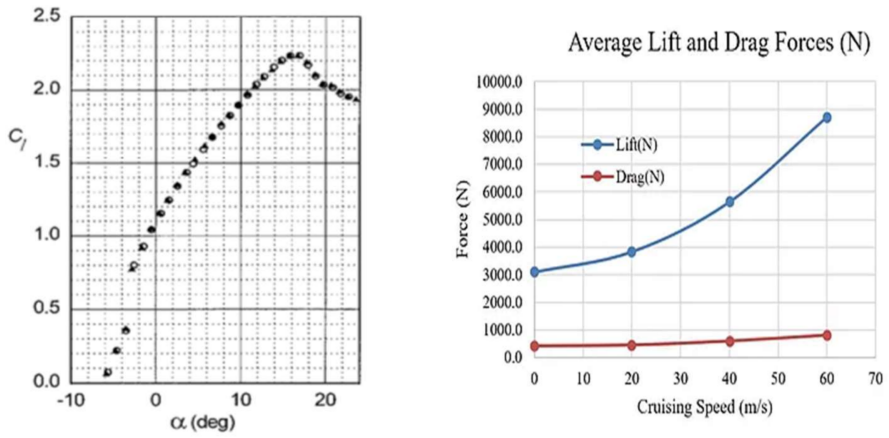

(**a**) (**b**)

Figure 8. (**a**) A plot of S1223 airfoil lift characteristics as a fixed airfoil. Reprinted from [16]; (**b**) The CFD aerodynamic results of lift/drag vs. cruise speeds for S1223 as a reciprocating wing of 1 m^2. Reprinted from [15].

The CFD simulation work was carried out for the S1223 airfoil by solving the governing equations (which include the continuity and momentum equations) to validate the performance of an RA-driven VTOL aircraft using the Ansys Fluent commercial code. The models available for the commercial CFD software's usage for turbulence calculations include the mixing length model, the Spalart–Allmaras model, k-ω model, k-ε model, the algebraic stress model, and the Reynolds stress model. The k-ε model is especially popular in simulating turbulent flow conditions and the types of the k-ε model include the standard k-ε model, the Renormalization Group (RNG) theory k-ε model, and the Realizable k-ε model. The turbulence model selected for the simulation was the Realizable k-ε model with enhanced wall function. The Realizable k-ε model can fulfill some mathematical constraints better than the standard k-ε and RNG k-ε models.

Figure 9a shows graphical simulation results of an S1223 wing during the forward stroke in a reciprocating wing cycle, and Figure 9b shows the reverse stroke in the reciprocating cycle. The dynamic simulation indicates that due to the positive AoA in both strokes, the lift is generated in both the forward and backward strokes, although the magnitude may differ. The meaningful lift for the design is the averaged lift over the entire cycle. At a zero-flight speed (takeoff), the lift coefficient, based on the life force and planform area of 1 m^2, as well as an average reciprocating speed of 50 m/s (180 km/h), is nearly 2.0 (Figure 8b). While at a cruise speed of 60 m/s (216 km/h), the lift coefficient based on the cruise speed and air density of 1.225 kg/m^3 is about 4.0. During the cruise, the forward speed of the aircraft would be superposed on the reciprocating speed of the wing. The implication is that the actual velocity across the wing is higher than 60 m/s (216 km/h) and the lift coefficient of 4.0 could be higher than the actual value. In this case, a more reliable gauge for the performance is the ratio of the lift force to the drag. According to Figure 8b at the takeoff, the ratio of lift to drag is above 7.3 while at the cruise speed of 60 m/s (216 km/h), it is above 10, indicating that the RA wing matches the performance of a fixed-wing without involving high-lift devices and greatly outperforms a corresponding rotary-wing. At takeoff, the results indicate a more than 70% reduction in power consumption per ton lift over rotary wings. The figure also shows that the cruise speed greatly improves the lift, which is almost tripled at a flight speed of 60 m/s (216 km/h) compared to the takeoff lift at the same reciprocating speed. The cruise speed of the aircraft creates airflow across the RA module to produce lift, and the need for the reciprocating motion of the RA module is reduced. Therefore, the reciprocating speed of the RA module can be gradually reduced to maintain the same lift. At a flight speed of about 240 km/h, the reciprocating motion of the RA module may be completely stopped to function as fixed wings. For a more detailed description of the CFD work, please see [15].

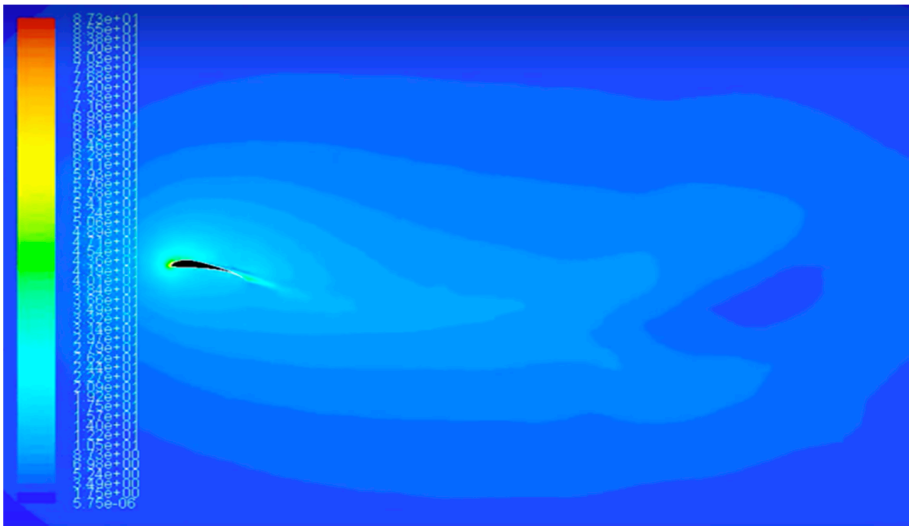

(**a**)

Figure 9. *Cont.*

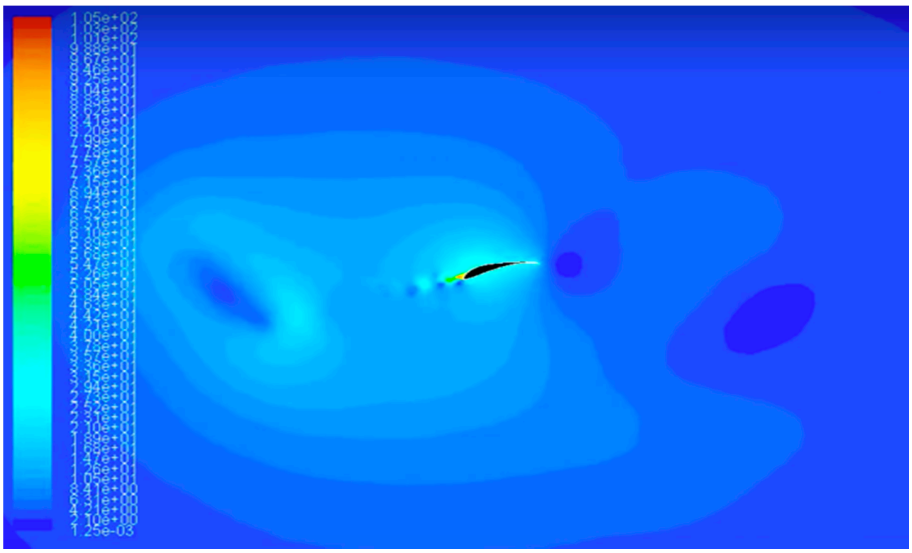

(**b**)

Figure 9. Dynamic computational simulation illustration of a reciprocating cycle: (**a**) Forward stroke with a positive AoA, and (**b**) backward stroke with a positive AoA.

3. Reciprocating Wing Design and Structural Analyses

Structural analyses are commonly utilized to test aircraft component systems to keep aircraft steady in the air as well as to predict the potential failure of the components. Proper analysis and interpretation of the results from structural analyses are essential for aircraft safety and overall performance.

3.1. Wing Structure

Our research goal was to design an effective wing for the RA module that matched the performance of fixed-wing aircraft. A major design requirement was the capability of the wing to structurally withstand the reciprocating inertia forces and to attain high lift, endurance, and range while also maintaining VTOL competencies. The first step of the design started with exporting the standard Selig S1223 airfoil profile coordinates to SolidWorks [19] to form the airfoil shape and the design processes continued from there. Table 2 shows the parameters used for the design of the wing. The use of ribs and spars increase the strength of a wing structure and the ribs preserve the shape of the airfoil and transmit the load to the spars. Together with the skin, the wing structure forms an efficient torsion partner. The planform area of the wing design was about 0.75 m^2, and the total mass was about 16.4 kg. The complete wing structure design with ribs, skin, and four spars, is shown in Figure 10.

Table 2. Wing design parameters.

Parameters	Characteristics
Wingspan (total) (m)	2
S1223 Airfoil chord length (c) (m) (center chord or wing root)	0.5
S1223 Airfoil chord length (c) (m) (wingtip)	0.25
Mass (kg)	16.4
Planform area (m^2)	0.75

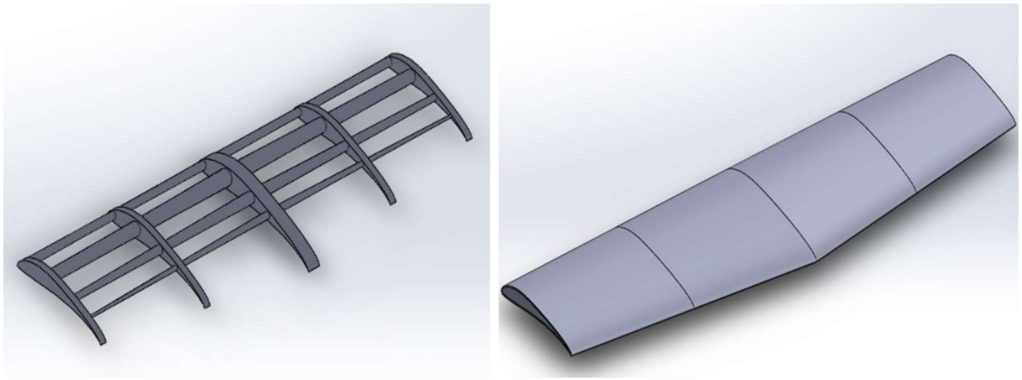

(**a**) (**b**)

Figure 10. (**a**) The internal structure of the wing and (**b**) complete wing structure.

3.2. Material Selection

Aircraft, in general, are sensitive to weight and the commonly preferred design yardstick of modern-day aircraft structure is weight minimization. Advanced composites in the aerospace industry have seen an increase in usage because of their high tensile strength and stiffness. Also, they are lightweight, tolerant to excessive heat, and resistant to corrosion and fatigue (meaning they do not easily form cracks with repeated loading). The last 50 years have witnessed a continued increase in the utilization of composites for aerospace applications, and the majority of UAVs are made from carbon fiber composites [20]. The material used for the design of the S1223 airfoil wing was high strength carbon fiber and its properties are given in Table 3 [21].

Table 3. Material Properties of high strength carbon fiber.

Properties	High Strength Carbon Fiber
Density ρ (g/cm^3)	1.58
Young's modulus (E) (MPa)	123,420
Bulk modulus (MPa)	121,000
Shear modulus (MPa)	46,397
Poisson's ratio (ν)	0.33
Tensile yield strength (MPa)	1723.7
Tensile ultimate strength (MPa)	3447.4
Compressive ultimate strength (MPa)	2413.2
Compressive yield strength (MPa)	1275.5

3.3. Boundary Conditions and Static Simulation Setup

Finite element analysis (FEA) is utilized for structural analyses and calculations of the stresses, displacements, and strains under the influence of a set of loads. ANSYS static structural solver [22] is used to perform the structural analyses, and the simulation setup usually involves the discretization, solving of the algebraic equations, application of the loads, and displaying the displacements, stresses, and strains results.

Figure 11a shows the meshing of the wing and Figure 11b shows the boundary conditions applied. It is well known that a sufficiently fine mesh is required for simulation results of acceptable accuracy. In this study, the mesh was set up with high smoothing, an internal body element size of 10 mm, and an external or face element size of 5 mm. The total number of nodes generated for the mesh was 1,257,183, while the total number of elements generated was 678,110. This setup ensured good static analysis results with the boundary conditions.

(**a**)

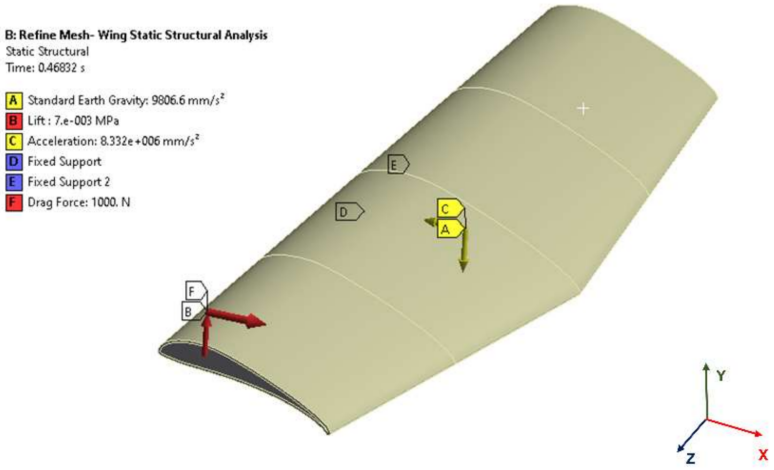

(**b**)

Figure 11. (**a**) The meshing of the wing and (**b**) boundary conditions applied to the wing.

Under real operational conditions during takeoff, the RA wing undergoes a reciprocating motion that is guided by a track through a pitch control mechanism. However, our structural analysis was based on a moving coordinate system that undergoes the same reciprocating motion of the RA wing. As a result, the wing under our analysis appeared to be stationary and was supported by a fixed pitch control mechanism. The boundary conditions included the fixed support (indicated in the setup as the connection to the pitch control mechanism, as shown in Figure 11b). To replicate this boundary condition in the FEA analysis, a portion underneath the wing area was fixed, which is where the pitch control mechanism would be installed. The other boundary conditions included a pressure force (F_{lift}), a gravity term (g), drag force (F_{drag}), and an acceleration term (x'') to account for the high inertia forces during the reciprocating mode of the wing. The acceleration term may be a function of time and is derived below in the results section. The specification of the acceleration term results in the inertia force condition to be imposed. A pressure force of 7000 N/m^2 acquired from the aerodynamic data was applied as the lift force, while a drag force of 1000 N was imposed based on the minimum ratio of the lift to drag of about 7.0.

4. Results and Discussions

Although the reciprocating wing may stop reciprocating and work as a fixed-wing during the cruise of the RA-driven VTOL drone, the wing structure analysis must be undertaken during the VTOL modes because of the very high inertia force loading in connection with the reciprocating motion of the wing. Since the wings are driven by a crankshaft system, the motion and acceleration/declaration of the wing are controlled by the crankshaft system, and a crank-slider mechanism is considered for this purpose. In this case, the wing would undertake the same reciprocating motion of the slider in the crank-slider mechanism, and the inertial forces of the wing will be directly related to the acceleration of the slider. The inertia body force related to the reciprocating motion of the wing may be specified by the acceleration term for the stress analyses. The parameters and equations used in deriving the acceleration are given below.

- Crank radius (r): 1 m (a 2 m reciprocating stroke of the wing)
- Connecting rod length (l): 2.85 m
- Crankshaft reciprocating frequency (f): 12.5 Hz (750 RPM)

For a cycle that includes two strokes (forward and reverse) with a reciprocating frequency of 12.5 Hz, the corresponding period is from 0 to 0.08 s, and the acceleration calculations are presented below:

The crankshaft angular velocity is given by Equation (1):

$$\begin{gathered} \omega = \frac{2\pi \cdot \mathrm{RPM}}{60} \cong 2\pi f \\ \omega = 78.54 \text{ rad/s} \end{gathered} \tag{1}$$

The acceleration in terms of the crankshaft rotating angle is given by Equation (2) below:

$$x'' = \left(-r \cdot \cos\ \theta - \frac{r^2 \cdot \left(\cos^2 \theta - \sin^2 \theta\right)}{\sqrt{l^2 - r^2 \cdot \sin^2 \theta}} - \frac{r^4 \cdot \sin^2 \theta \cdot \cos^2 \theta}{\left(\sqrt{l^2 - r^2 \cdot \sin^2 \theta}\right)^3} \right) \omega^2 \tag{2}$$

But the angle can be related to the time:

$$\theta = \omega t \tag{3}$$

Therefore,

$$x'' = \left(-r \cdot \cos\ \omega t - \frac{r^2 \cdot \left(\cos^2 \omega t - \sin^2 \omega t\right)}{\sqrt{l^2 - r^2 \cdot \sin^2 \omega t}} - \frac{r^4 \cdot \sin^2 \omega t \cos^2 \omega t}{\left(\sqrt{l^2 - r^2 \cdot \sin^2 \omega t}\right)^3} \right) \omega^2 \tag{4}$$

The acceleration, a, as a function of time, is, therefore:

$$a = x'' \tag{5}$$

Using the equations above, the inertia body-force-related accelerations of the RA wing for static analyses were between 4004 m/s^2 and -8332 m/s^2, and a maximum acceleration magnitude of 8332 m/s^2 was applied along the longitudinal direction of the wing for one stroke with the same AoA.

With the applied boundary conditions and inertia body forces, FEA using ANSYS static structural solver were carried out, and the results in terms of the total deformations, equivalent (von Mises) stress, and equivalent strain of the wing under the loading conditions were obtained. Figure 12a–c, respectively, show the total deformation, the equivalent (von Mises) stress, and the equivalent strain simulation plots of the wing. Finite element analyses, with the lift loading but without the inertia force specification, were also undertaken, and the maximum total deformation, equivalent (von Mises) stress, and equivalent

strain values, together with those including the inertia force specification are summarized in Table 4. As shown in the Table, the inertia force loading due to the reciprocating motion of the wing dominates the results of the structural analyses. With the inertia force loading, the maximum total deformation, equivalent (von Mises) stress, and equivalent strain values were 1.73 mm, 309.14 MPa, and 0.0027824 mm, respectively.

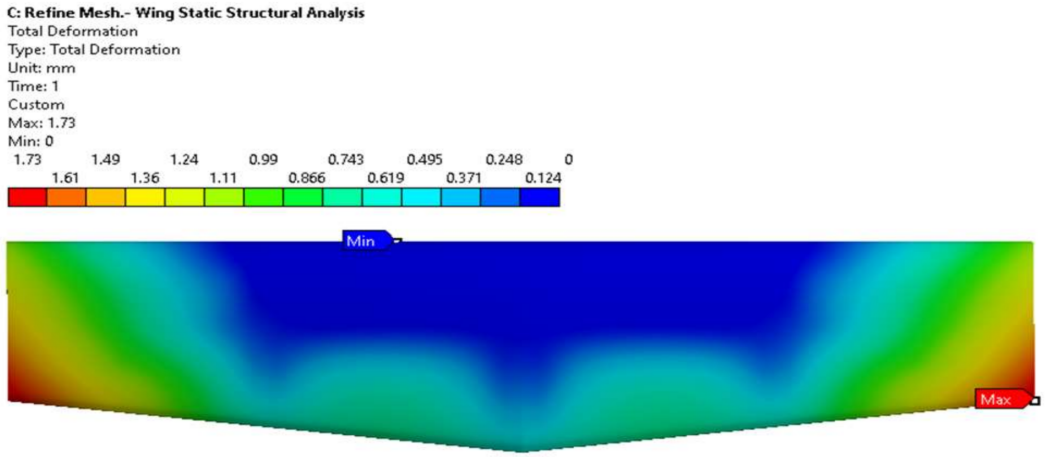

(**a**)

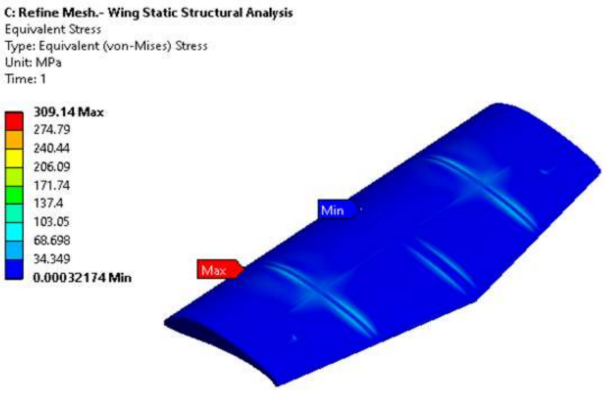

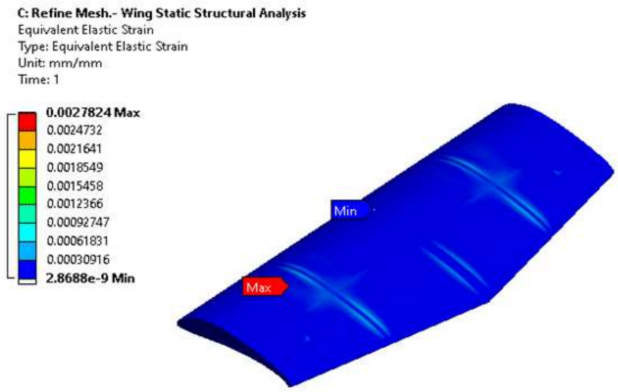

(**b**) (**c**)

Figure 12. (**a**) Total deformation, (**b**) Equivalent (von Mises) stress, and (**c**) Equivalent elastic strain.

Table 4. Maximum deformation, stress, and strain with and without inertia force specification.

Case	Total Deformation (mm)	Equivalent (Von Mises) Stress (MPa)	Equivalent Elastic Strain (mm)
Without inertia force	0.19098	35.309	0.00039788
With inertia force	1.73	309.14	0.0027824

The question is: Are the results above acceptable to the designed wing structure herein? Stress analysis is seen as the best measure to determine the amount of potential damage a model can handle after the application of the load. One commonly used and efficient way of answering the question is to take the scalar von Mises stress (MPa) and directly compare it with the yield strength of the chosen material. This can give us an idea of the range of potential failure of the model. The value from the yield strength of our material was about 1723.7 MPa and it was compared directly with the outcome of the stress results from the simulation of 309.14 MPa. Although the value of the equivalent stress seems high compared to the tensile yield strength of the material, this stress result is considered to be within an acceptable stress range. Further studies will focus on various configurations and structural optimization to improve the stress condition of the RA wing.

5. Conclusions

The state-of-the-art of VTOL UAV is briefly reviewed, including RA-driven VTOL aircraft. It is believed that the high lift capability during takeoff and the smooth and natural transition to the fixed-wing operation make the RA VTOL UAVs attractive as compared to other VTOL UAVs.

The selection of the Selig S1223 airfoil profile proved to be an excellent choice for this RA-driven VTOL UAV model application due to its superior performance at low Reynolds numbers, high-lift, and reduced noise characteristics at low AoA.

Advanced composites usage is expected to burgeon in aircraft and UAV applications because of their high stiffness and major lightweight advantage over other materials. Utilizing high-strength carbon fiber as the selected material of the wing design contributed to weight minimization and minimal deformation of the RA wing.

The primary motion of the RA module is a linear reciprocating motion driven by a crank-slider mechanism, which generates strong inertia body force in the wing structure and represents a significant challenge to the wing design. Compared to the case without inertia force, our structural analysis detected much higher von Mises stresses after the inertia loading was imposed. However, compared to the tensile yield strength of the material, the stress result was satisfactory. Additionally, the maximum deformation and strain values were all within an acceptable range and no material failures were detected.

The results of this study indicate that the reciprocating wing could survive the strong inertia forces and its use in an RA-driven aircraft appears feasible. Future work will further validate the proposed methodology with various configurations to improve the stress condition of the wing for weight minimization. Fatigue analysis and second law studies may also be undertaken in the future.

Author Contributions: Conceptualization, J.O.I. and Y.C.; methodology, J.O.I.; software, J.O.I. and M.D.A.; validation, J.O.I., Y.C. and M.D.A.; formal analysis, J.O.I. and Y.C.; investigation, J.O.I. and M.D.A.; writing—original draft preparation, J.O.I.; writing—review and editing, J.O.I. and Y.C.; visualization, J.O.I. and M.D.A.; supervision, Y.C.; project administration, Y.C. All authors have read and agreed to the published version of the manuscript.

Funding: This research received no external funding.

Institutional Review Board Statement: Not applicable.

Informed Consent Statement: Not applicable.

Data Availability Statement: Not applicable.

Acknowledgments: The authors would like to thank Soheil Soleimanikutanaei and Esmaiil Ghasemisahebi for their work on the computational analyses of the reciprocating airfoil.

Conflicts of Interest: The authors declare no conflict of interest.

Nomenclature

Symbols	
$C_{L\,max}$	Maximum Airfoil Coefficient of Lift
$C_{m,c/4}$	Airfoil pitching-moment coefficient about the quarter-chord point
α_{max}	Maximum Angle of Attack (AoA)
c	Airfoil chord length
F_{Lift}	Lift Force
F_{drag}	Drag Force
ν	Poisson's Ratio
ω	Crankshaft Angular Velocity
f	Crankshaft Reciprocating Frequency
t	Time
r	Crank Radius
l	Connecting Rod Length
θ	Crankshaft Rotating Angle
x''	Acceleration term
g	Gravity term
Acronyms and abbreviations	
VTOL	Vertical Takeoff and Landing
UAV	Unmanned Aerial Vehicle
CTOL	Conventional Takeoff and Landing
RA	Reciprocating Airfoil
CFD	Computational Fluid Dynamics
FEA	Finite Element Analysis
NACA	National Advisory Committee for Aeronautics

References

1. Airbus. VSR700. Available online: www.airbus.com/helicopters/UAS/VSR700.html (accessed on 9 June 2021).
2. Northrop Grumman. Fire Scout. Available online: www.northropgrumman.com/what-we-do/air/fire-scout (accessed on 10 June 2021).
3. Northrop Grumman. Global Hawk Enterprise. Available online: www.northropgrumman.com/what-we-do/air/global-hawk-enterprise/#records-and-awards (accessed on 10 June 2021).
4. General Atomics Aeronautical Systems Inc. MQ-9A "Reaper" (Predator B). Available online: https://www.ga-asi.com/remotely-piloted-aircraft/mq-9a (accessed on 2 May 2021).
5. Ozdemir, U.; Aktas, Y.O.; Vuruskan, A.; Dereli, Y.; Tarhan, A.F.; Demirbag, K.; Erdem, A.; Kalaycioglu, G.D.; Ozkol, I.; Inalhan, G. Design of a commercial hybrid VTOL UAV system. *J. Intell. Robot. Syst.* **2014**, *74*, 371–393. [CrossRef]
6. Çetinsoy, E.; Dikyar, S.; Hançer, C.; Oner, K.T.; Sirimoglu, E.; Unel, M.; Aksit, M.F. Design and construction of a novel quad tilt-wing UAV. *Mechatronics* **2012**, *22*, 723–745. [CrossRef]
7. Czyba, R.; Lemanowicz, M.; Gorol, Z.; Kudala, T. Construction prototyping, flight dynamics modeling, and aerodynamic analysis of hybrid VTOL unmanned aircraft. *J. Adv. Transp.* **2018**, *2018*, 7040531. [CrossRef]
8. Flores-Colunga, G.R.; Lozano-Leal, R. A nonlinear control law for hover to level flight for the quad tilt-rotor uav. *IFAC Proc. Vol.* **2014**, *47*, 11055–11059. [CrossRef]
9. Aktas, Y.O.; Ozdemir, U.; Dereli, Y.; Tarhan, A.F.; Cetin, A.; Vuruskan, A.; Yuksek, B.; Cengiz, H.; Basdemir, S.; Ucar, M.; et al. Rapid prototyping of a fixed-wing VTOL UAV for design testing. *J. Intell. Robot. Syst.* **2016**, *84*, 639–664. [CrossRef]
10. Hochstenbach, M.; Notteboom, C.; Theys, B.; de Schutter, J. Design and control of an unmanned aerial vehicle for autonomous parcel delivery with transition from vertical take-off to forward flight–vertikul, a quadcopter tailsitter. *Int. J. Micro Air Veh.* **2015**, *7*, 395–405. [CrossRef]
11. Orbea, D.; Moposita, J.; Aguilar, W.G.; Paredes, M.; Reyes, R.P.; Montoya, L. Vertical take off and landing with fixed rotor. In Proceedings of the 2017 CHILEAN Conference on Electrical, Electronics Engineering, Information and Communication Technologies (CHILECON), Pucon, Chile, 18–20 October 2017; IEEE: Piscataway, NJ, USA, 2017; pp. 1–6.
12. Çakici, F.; Leblebicioğlu, K.M. Control system design of a vertical take-off and landing fixed-wing UAV. *IFAC Pap.* **2016**, *49*, 267–272. [CrossRef]
13. Lockheed Martin. SB > 1 DEFIANT^{TM}. Available online: https://www.lockheedmartin.com/en-us/products/sb1-defiant-technology-demonstrator.html (accessed on 2 May 2021).
14. Cao, Y. Reciprocating Lift and Thrust Systems. U.S. Patent Application 16/967200, 4 August 2020.
15. Cao, Y. Reciprocating-Airfoil (RA) Driven VTOL Aircraft. 2019. Available online: https://www.congruityaerospace.com/ (accessed on 15 January 2021).
16. Selig, M.S.; Guglielmo, J.J. High-lift low Reynolds number airfoil design. *J. Aircraft.* **1997**, *34*, 72–79. [CrossRef]

17. Oller Aramayo, S.A.; Nallim, L.G.; Oller Martínez, S.H. The usability of the Selig S1223 profile airfoil as a high lift hydrofoil for hydrokinetic application. *J. Appl. Fluid Mech.* **2016**, *9*, 537–542.
18. Ma, R.; Liu, P. Numerical simulation of low-Reynolds-number and high-lift airfoil S1223. In Proceedings of the World Congress on Engineering, London, UK, 1–3 July 2009; Volume 2, pp. 1–3.
19. SolidWorks, D.S.; SolidWorks®. Version 2019. Available online: https://www.solidworks.com/ (accessed on 28 January 2021).
20. Hexcel. Unmanned Aerial Vehicles (UAVs). Available online: https://www.hexcel.com/Resources/UAV (accessed on 2 May 2021).
21. Granta. ANSYS Granta EduPack-Materials Data for Simulation. 2019. Available online: https://www.ansys.com/products/materials/granta-edupack (accessed on 2 April 2021).
22. ANSYS. ANSYS Workbench Static Structural—CFD Software | ANSYS (2019). Available online: https://www.ansys.com/products/structures/ansys-mechanical (accessed on 2 April 2021).